



## Detection of SiO emission from a massive dense cold core

**Author:**

Lo, N; Cunningham, Maria; Bains, Indra; Burton, Michael; Garay, Guido

**Publication details:**

Monthly Notices of the Royal Astronomical Society - Letters

v. 381

Chapter No. 1

pp. L30-L34

1745-3933 (ISSN)

**Publication Date:**

2007

**Publisher DOI:**

<http://dx.doi.org/10.1111/j.1745-3933.2007.00360.x>

**License:**

<https://creativecommons.org/licenses/by-nc-nd/3.0/au/>

Link to license to see what you are allowed to do with this resource.

Downloaded from <http://hdl.handle.net/1959.4/38590> in <https://unsworks.unsw.edu.au> on 2024-04-20

# Detection of SiO emission from a massive dense cold core

N. Lo,<sup>1,2\*</sup> M. Cunningham,<sup>1</sup> I. Bains,<sup>1,3</sup> M. G. Burton<sup>1</sup> and G. Garay<sup>4</sup>

<sup>1</sup>*School of Physics, University of New South Wales, Sydney, NSW 2052, Australia*

<sup>2</sup>*Australia Telescope National Facility, CSIRO, PO Box 76, Epping, NSW 1710, Australia*

<sup>3</sup>*Centre for Astrophysics and Supercomputing, Swinburne University of Technology, P.O. Box 218, Hawthorn, VIC 3122, Australia*

<sup>4</sup>*Departamento de Astronomía, Universidad de Chile, Casilla 36-D, Santiago, Chile*

Accepted \*\*\*. Received \*\*\*; in original form \*\*\*

## ABSTRACT

We report the detection of the SiO ( $J = 2 \rightarrow 1$ ) transition from the massive cold dense core G333.125–0.562. The core remains undetected at wavelengths shorter than 70- $\mu$ m and has compact 1.2-mm dust continuum. The SiO emission is localised to the core. The observations are part of a continuing multi-molecular line survey of the giant molecular cloud G333. Other detected molecules in the core include  $^{13}\text{CO}$ ,  $\text{C}^{18}\text{O}$ , CS,  $\text{HCO}^+$ , HCN, HNC,  $\text{CH}_3\text{OH}$ ,  $\text{N}_2\text{H}^+$ , SO,  $\text{HC}_3\text{N}$ ,  $\text{NH}_3$ , and some of their isotopes. In addition, from  $\text{NH}_3$  (1,1) and (2,2) inversion lines, we obtain a temperature of 13 K. From fitting to the spectral energy distribution we obtain a colour temperature of 18 K and a gas mass of  $2 \times 10^3 M_\odot$ . We have also detected a 22-GHz water maser in the core, together with methanol maser emission, suggesting the core will host massive star formation. We hypothesise that the SiO emission arises from shocks associated with an outflow in the cold core.

**Key words:** Radio lines: ISM - ISM: clouds - ISM: molecules - ISM: structure - ISM: dust, extinction - stars: formation.

## 1 INTRODUCTION

### 1.1 Dense cold core G333.125–0.562

The massive, dense, cold core G333.125–0.562 ( $\alpha_{J2000} = 16^{\text{h}}21^{\text{m}}35^{\text{s}}$ ,  $\delta_{J2000} = -50^{\text{d}}41^{\text{m}}10^{\text{s}}$ ) is located in one of the southern massive star forming region, G333 Giant Molecular Cloud complex at a distance of 3.6-kpc. It has a dust mass of  $2.3 \times 10^3 M_\odot$  and a density of  $2 \times 10^5 \text{ cm}^{-3}$  (Garay et al. 2004). The cold core was discovered by Garay et al. (2004), comparing the SEST Imaging Bolometre Array (SIMBA) 1.2-mm survey (Faúndez et al. 2004) with *Midcourse Space Experiment (MSX)* mid-infrared data and *Infrared Astronomical Satellite (IRAS)* far-infrared data. Garay et al. noted strong 1.2-mm continuum emission from this source in the absence of emission in any of the *MSX* and *IRAS* bands. From the 1.2-mm dust continuum, along with the upper limits of *IRAS* fluxes, they inferred that the core is extremely cold ( $< 17$  K), massive and dense. Garay et al. hypothesised that the core is at an early stage of star formation, most likely before the development of an internal luminosity source, and will collapse to form high-mass star(s).

Pestalozzi et al. (2002) conducted SIMBA 1.2-mm observations of the source based on the detection of a class II 6.6-GHz methanol maser from survey by the Mt Pleasant

Observatory (Ellingsen et al. 1996). Pestalozzi et al. suggested that there is a very deeply embedded object because of the detection of strong 1.2-mm emission and the methanol maser. Later, a class I 95.1-GHz methanol was detected by Ellingsen (2005) with the Mopra Telescope.

## 2 OBSERVATIONS AND DATA PROCESSING

The multi-molecular line data presented here were collected between July 2004 and October 2006 with the Mopra Telescope, operated by the Australia Telescope National Facility (ATNF). It has a full width half-maximum (FWHM) beam size of  $\sim 32$  arcsec at 100-GHz (Ladd et al. 2005). The observations were carried out with the new UNSW Mopra Spectrometer (MOPS) digital filterbank back-end and Monolithic Microwave Integrated Circuit (MMIC) receiver, except for  $^{13}\text{CO}$  and  $\text{C}^{18}\text{O}$  which were observed with the Mopra Correlator (MPCOR) and the previous Superconductor Insulator Superconductor (SIS) receiver (Bains et al. 2006). According to Ladd et al. (2005) the main beam efficiency at 86-GHz is 0.49, and at 115-GHz is 0.42.

The observations are part of the on-going multi-molecular line survey (the ‘Delta Quadrant Survey’ or DQS) project carried out by the University of New South Wales, of the giant molecular cloud complex G333. The cold core

\* E-mail: nlo@phys.unsw.edu.au

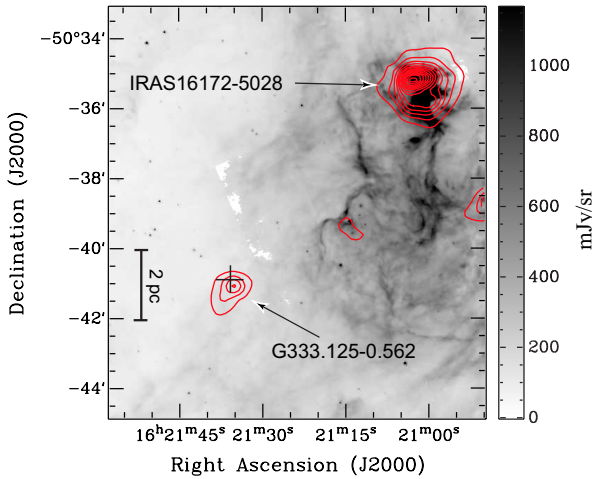


**Figure 1.** GLIMPSE 8- $\mu$ m image (grey scale) overlaid with the SIMBA 1.2-mm dust continuum (red contours). The contour levels start from 690 mJy beam $^{-1}$  with increments of 690 mJy beam $^{-1}$ . The arrows show the position of the core and the IRAS source, the cross shows the 6.7-GHz methanol maser, while the scale bar denotes 2-pc at a distance of 3.6-kpc. No 8- $\mu$ m emission is evident at the position of the core.

G333.125–0.562 is part of the complex. The first paper featuring  $^{13}\text{CO}$  is already published (Bains et al. 2006). In addition to the 3-mm multi-molecular line survey,  $\text{NH}_3$  and  $\text{H}_2\text{O}$  (12-mm) maps of the core were also obtained during December 2006 with the Mopra Telescope. The main beam efficiency for 12-mm system is  $\eta_{22\text{GHz}} = 0.7$  and FWHM beam size approximately 2 arcmin. The data presented in this work has a pointing accuracy of within  $\sim 5$  arcsec.

### 3 RESULTS AND DISCUSSIONS

Shown in Figure 1 is the *Spitzer* Galactic Legacy Infrared Midplane Survey Extraordinaire (GLIMPSE) 8- $\mu$ m image (grey scale) overlaid with the SIMBA 1.2-mm dust continuum (red contours) obtained from Mookerjee et al. (2004). From the image it can be seen that the core (bottom left) is isolated and has compact dust emission. No infrared emission is evident from it. Inspection of the *Spitzer* MIPS GAL images at 24- and 70- $\mu$ m show a source only at the longer wavelength. Thus this must be a cold dust core. From this core we have further detected emission from a number of molecular transitions, their observed parameters are summarised in Table 1. Among these, the detection of SiO ( $J = 2 \rightarrow 1$ ) is of particular interest. Presented in Figure 2 is the integrated emission map of SiO (red contours) overlaid on CS (grey scale), both maps have been smoothed to 36 arcsec. From the map we can see there are two strong peaks of SiO emission, one is the luminous IRAS source IRAS16172–5028 and the other one is from the cold, dense core G333.125–0.562. This is quite different to the extended distribution seen in other molecular transitions in this region. Shown in the inset is the SiO velocity profile averaged over the core (dashed box), it is evident the line profile is broad. We will first discuss the distribution of the molecules, followed by the physical properties derived for the core.

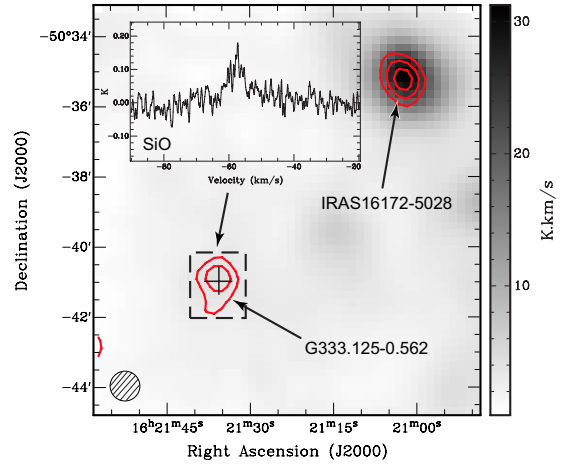


**Figure 2.** The integrated emission map of SiO  $J = 2 \rightarrow 1$  transition (red contours) overlaid on CS  $J = 2 \rightarrow 1$  transition (grey scale). The contour levels start from 1.2 K km $^{-1}$  in steps of 0.4 K km $^{-1}$  ( $1\sigma$ ), in terms of the antenna temperature,  $T_A^*$ . The cross shows the 6.7-GHz methanol maser, the hatched circle indicates the beam size. The inset is the velocity profile of SiO averaged over the region indicated by the dashed box.

#### 3.1 Distribution of the molecules

Presented in Figure 3 are the integrated emission (zeroth moment) maps of the detected molecular lines over velocity range of  $-80$  to  $-40$  km s $^{-1}$ , except  $^{13}\text{CO}$  and  $\text{C}^{18}\text{O}$ , which are integrated over the ranges indicated in the figure. The molecular line emission peaks are coincident (within a beam) with the 1.2-mm dust, except for  $\text{C}^{18}\text{O}$  which is offset by approximately 55 arcsec ( $\sim 1$ -pc at a distance of 3.6-kpc). Note that there is extended  $\text{C}^{18}\text{O}$  emission towards the north of the dust peak. The low density tracer CO is clearly more extended than the other molecules, which are sensitive to denser gas. Recent studies (Lintott et al. 2005) suggest that CS is a good tracer of dense cores in high-mass star forming regions in contrast to low-mass star formation where CS may be depleted. Since the peak matches well with the dust peak, this suggests that CS does not suffer from significant depletion. However, we do note that depletion could happen at smaller scales. Another feature evident in the HNC and  $\text{HCO}^+$  maps is the tongue of extended emission to the south-west (arrow). A comparison between HCN and HNC integrated emission maps shows large differences in distribution, HCN being more extended than HNC, while at the same time the peak brightness of HCN is lower than HNC. Whether this is caused by optical depth effects needs further investigation. Although HCN and HNC have the same precursors ( $\text{HCNH}^+$  and  $\text{H}_2\text{CN}^+$ ) and similar dipole moments, it is believed that HCN is enhanced in warm environments in contrast to HNC, which forms preferentially in colder conditions (Kim et al. 2006). Hirota et al. (1998) found the abundance ratio of  $[\text{HNC}]/[\text{HCN}]$  rapidly drops as the temperature exceeds a temperature of 24-K.  $\text{N}_2\text{H}^+$  is known as a cold gas tracer as its abundance tends to be enhanced in cold dense cores, due to the depletion of CO, which decreases the destruction of  $\text{N}_2\text{H}^+$  and  $\text{H}_3^+$  (Womack, Ziurys & Wyckoff 1992; Hotzel, Harju & Walmsley 2004). Rather than reacting with CO to form  $\text{HCO}^+$  and  $\text{H}_2$ , the  $\text{H}_3^+$  ion reacts with  $\text{N}_2$  to form  $\text{N}_2\text{H}^+$ . From the integrated emission

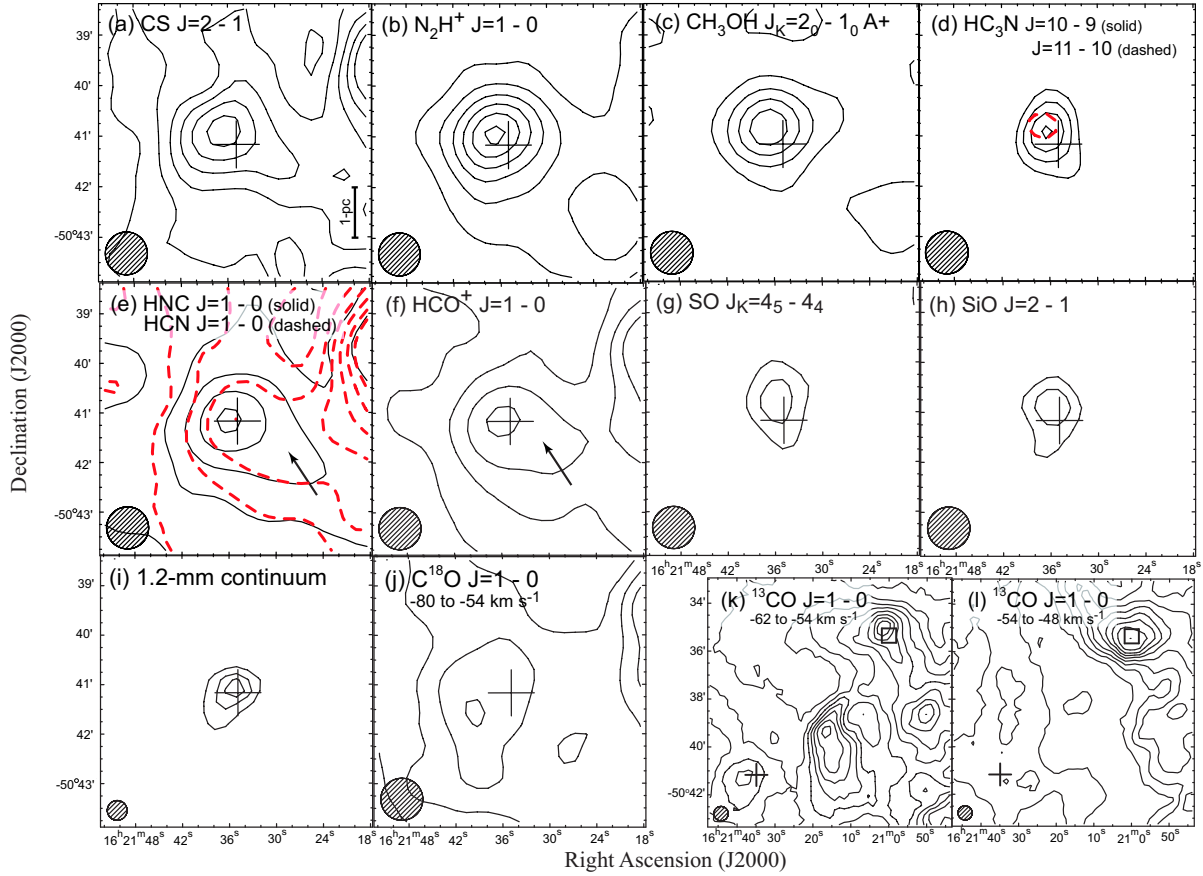


**Figure 3.** (a) to (j): Integrated emission maps of various molecular lines, as indicated for the core G333.125–0.562. The contour levels start from  $3\sigma$  of the r.m.s. The contour levels of  $\text{N}_2\text{H}^+$ ,  $\text{CH}_3\text{OH}$ ,  $\text{HNC}$ ,  $\text{HCN}$ ,  $\text{HCO}^+$ ,  $\text{C}^{18}\text{O}$  and 1.2-mm continuum are in steps of  $3\sigma$ , and  $1\sigma$  for  $\text{CS}$ ,  $\text{HC}_3\text{N}$  (both transitions),  $\text{SO}$  and  $\text{SiO}$ . The r.m.s. for  $\text{CS}$  and  $\text{CH}_3\text{OH}$  is  $1.1\text{ K km s}^{-1}$ ,  $\text{N}_2\text{H}^+$  is  $0.91$ ,  $\text{HNC}$ ,  $\text{HCO}^+$  and  $\text{SiO}$  are  $0.82\text{ K km s}^{-1}$ ,  $\text{HC}_3\text{N}$  ( $J = 10 - 9$ ) and  $\text{HCN}$  are  $0.61\text{ K km s}^{-1}$ ,  $\text{HC}_3\text{N}$  ( $J = 11 - 10$ ) and  $\text{SO}$  is  $0.91\text{ K km s}^{-1}$ , and  $\text{C}^{18}\text{O}$  is  $1.2\text{ K km s}^{-1}$ . The integrated velocity range is from  $-80$  to  $-40\text{ km s}^{-1}$ , except  $\text{C}^{18}\text{O}$  which is from  $-80$  to  $-54\text{ km s}^{-1}$ . The arrows show the tongue extended emission in the south-west direction. (k):  $^{13}\text{CO}$  integrated emission map from  $-62$  to  $-54\text{ km s}^{-1}$ , over a region covers the core (lower left) and IRAS16172-5028 (upper right). (l): Same as figure k but over velocity range  $-54$  to  $-48\text{ km s}^{-1}$ . Contour levels for  $^{13}\text{CO}$  maps start from 20 per cent of the peak, in increments of 10 per cent. The cross marks the peak of the 1.2-mm continuum and the square is the UCHII region associated with IRAS 16172–5028. The beam sizes are indicated with the hatched circle, the scale bar denotes 1-pc at distance of 3.6-kpc.

map of  $\text{N}_2\text{H}^+$ , we see a compact distribution of  $\text{N}_2\text{H}^+$ . This suggests the  $\text{N}_2\text{H}^+$  is tracing the outer cold envelope of the dense core. The other two molecules which show a compact distribution are  $\text{CH}_3\text{OH}$  and  $\text{HC}_3\text{N}$  (both transitions), both of which trace dense gas.  $\text{SiO}$  and  $\text{SO}$  are known to be greatly enhanced in outflows and shocked regions (Martin-Pintado, Bachiller & Fuente 1992). Detecting both these species suggests that energetic activity associated with shock waves is present.

### 3.2 Physical properties

In order to derive the physical parameters, spectra were spatially averaged over the FWHM angular size for molecules with compact emission, otherwise over a  $48\text{ arcsec}$  region, then fitting with a Gaussian in CLASS<sup>1</sup>. The fitted param-

eters, i.e. line width, centre velocity, brightness temperature and optical depth (from hyperfine structure fitting of  $\text{N}_2\text{H}^+$  and  $\text{NH}_3$ ) were then used to derive column densities and masses. The derived parameters are summarised in Table 1. The column densities were calculated with an excitation temperature of  $15\text{ K}$ , which is the average of the dust and  $\text{NH}_3$  values (see below). We note that the derived column densities vary by 20 per cent for the excitation temperature range ( $13 - 18\text{ K}$ ). We have derived molecular abundances relative to the  $\text{H}_2$  column density, which is obtained from the 1.2-mm dust continuum,  $N_{\text{H}_2} \sim 4 \times 10^{23}\text{ cm}^{-2}$ .

From the  $\text{NH}_3$  ( $J,K$ ) = (1,1) and (2,2) inversion transitions we have calculated the rotational temperature ( $T_{12}$ ) of the core, following the method stated in Ungerechts, Winnewisser & Walmsley (1986). We assumed  $\text{NH}_3$  (1,1) and (2,2) are tracing the same volume of gas, and all hyperfine components have the same excitation temperature. With the above assumptions, we have derived the rotational temperature,  $T_{12} = 13.1\text{ K}$ , with an uncertainty range of  $12.9 - 13.3\text{ K}$ . According to Danby et al. (1988), below  $20\text{ K}$  the rota-

<sup>1</sup> Continuum and Line Analysis Single-dish Software, part of GILDAS software package by IRAM.  
(<http://www.iram.fr/IRAMFR/GILDAS/>)

**Table 1.** Summary of the observed and derived parameters of the molecular lines: centre velocity ( $V$ ), line width ( $\Delta V$ ), peak brightness ( $T_{\text{peak}}$ ), integrated brightness ( $\int T_{\text{MB}} dv$ ), isotopic column density ( $N$ ), virial mass ( $M_{\text{vir}}$ ) and FWHM angular size ( $\theta$ ). The second last column is the abundance ratio ( $X$ ) of the molecular line relative to  $\text{H}_2$ . For lines with more than one velocity component, parameters reported here are for the component associated with the core velocity,  $-58 \text{ km s}^{-1}$ . The uncertainty range is in parentheses.

Molecule	Transition	$V$ ( $\text{km s}^{-1}$ )	$\Delta V$ ( $\text{km s}^{-1}$ )	$T_{\text{peak}}$ (K)	$\int T_{\text{MB}} dv$ ( $\text{K km s}^{-1}$ )	$N$ ( $10^{14} \text{ cm}^{-2}$ )	$M_{\text{vir}}$ ( $10^3 M_{\odot}$ )	$\theta$ (arcsec)	$X$ ( $10^{-10}$ )	Note
<b>3-mm</b>										
$^{13}\text{CO}$	1 – 0	−57.56 (0.03)	4.90 (0.06)	9.5	49.3 (0.8)	$2.0 \times 10^3$	1.2	48	$5.0 \times 10^4$	[ex]
$\text{C}^{18}\text{O}$	1 – 0	−56.63 (0.05)	5.1 (0.1)	2.6	14.1 (0.3)	$5.2 \times 10^3$	1.3	48	$1.3 \times 10^4$	[ex]
CS	2 – 1	−58.8 (0.3)	4.5 (0.7)	0.9	4.1 (1.3)	1.7	1.0	48	4.3	[ex]
$\text{C}^{34}\text{S}$	2 – 1	−57.7 (0.3)	3.1 (0.8)	0.3	1.0 (0.2)	0.6	0.5	54	1.5	[c]
$\text{HCO}^+$	1 – 0	−59.4 (0.1)	4.6 (0.1)	2.1	10.4 (0.4)	2.7	1.1	48	6.8	[ex]
HCN	1 – 0									[hf]
	F = 2 – 1	−59.5 (0.1)	2.2 (0.3)	0.6	1.4 (0.2)	—	—	—	—	—
	F = 0 – 1	−66.6 (0.1)	5.3 (0.4)	0.7	3.9 (0.3)	—	—	—	—	—
	F = 1 – 1	−51.8 (0.4)	—	—	—	—	—	—	—	[I]
HNC	1 – 0	−59.07 (0.05)	3.9 (0.1)	2.2	9.2 (0.5)	$> 3 \times 10^{-3}$	0.8	46	$> 9 \times 10^{-3}$	[II]
$\text{N}_2\text{H}^+$	1 – 0	−58.8 (0.1)	4.0 (0.1)	1.0	3.9 (0.3)	24	3.3	99	61	[hf,c]
$\text{CH}_3\text{OH}$	$2_{02} - 1_{01} \text{ A}+$	−58.0 (0.1)	4.2 (0.2)	1.2	5.2 (0.3)	—	—	84	—	[c,III]
HCCCN	11 – 10	−57.3 (0.2)	3.6 (0.5)	0.3	1.3 (0.2)	0.6	1.3	69	1.5	[c,IV]
HCCCN	10 – 9	−57.41 (0.09)	3.8 (0.2)	0.6	2.5 (0.1)	—	—	—	—	[c]
SO	$3_2 - 2_1$	−57.2 (0.2)	5.0 (0.5)	0.5	2.7 (0.2)	1.1	1.3	48	2.6	[II]
SiO	$2 - 1 \text{ v}=0$	−57.2 (0.3)	9.0 (1.0)	0.2	1.8 (0.2)	4.4	3.9	48	11	[II]
<b>12-mm</b>										
$\text{NH}_3$	(1, 1)	−56.89 (0.02)	3.46 (0.03)	0.9	10.7 (0.2)	0.4	1.5	120	1	[hf,V]
$\text{NH}_3$	(2, 2)	−57.2 (0.1)	3.7 (0.2)	0.4	2.7 (0.2)	—	—	—	—	[hf]
$\text{H}_2\text{O}$	$6_{16} - 5_{23}$	−53.9 (0.1)	2.0 (0.3)	0.1	0.24 (0.03)	—	—	—	—	[m]

NOTE –

[hf] stands for hyperfine structures; the peak brightness is for the main component, and the integrated brightness for the sum of all hyperfine components, except HCN, which we list each hyperfine component.

[m] stands for maser.

[ex] indicates the molecular line emission is extended, hence we used the angular size of dust continuum to derive the virial mass.

[c] for compact emission.

[el] indicates the emission is elongated, the angular size is the average of RA and DEC.

[I] hyperfine component is blended with the  $-50 \text{ km s}^{-1}$  velocity component.

[II] we derived the column density assuming the line is optically thin, hence it and the abundance ratio are lower limits.

[III] no other  $\text{CH}_3\text{OH}$  transition detected, therefore column density cannot be calculated.

[IV] column density calculated using the rotational temperature (5.7-K) obtained from  $J = 10 \rightarrow 9$  and  $J = 11 \rightarrow 10$  lines.

[V] the beam size at 22-GHz is  $\sim 2$  arcmin, therefore the source is unresolved. We took the angular size to be one beam width as there is no noticeable extended emission.

tional temperature of  $\text{NH}_3$  (1,1)-(2,2) matches the kinetic temperature ( $T_{\text{kin}}$ ) well.

We are also able to determine a dust temperature, mass and luminosity from the spectral energy distribution (SED). Inspection of the GLIMPSE and MIPS GAL images of the core only shows evidence of emission at the longest wavelength (70- $\mu\text{m}$ ). Far-IR balloon-borne measurements have been made at 150 and 210- $\mu\text{m}$  by Karnik et al. (2001), through a 3 arcmin beam. Examination of the *Spitzer* infrared images show this emission must be confined to the G333.125–0.562 core. Hence we use the 150-, 210- $\mu\text{m}$  and 1.2-mm fluxes to determine the SED, constraining the size by the angular size (48 arcsec) of the 1.2-mm core, and applying a greybody fit with a dust emissivity index of  $\beta = 2$  (Hill et al. 2006). This yields the following parameters for the core:  $T_{\text{dust}} = 18.6 \pm 0.1 \text{ K}$ ,  $L_{\text{bol}} = (8.5 \pm 0.3) \times 10^3 L_{\odot}$  and  $M_{\text{gas}} = 1.8 \times 10^3 M_{\odot}$ . Taken with the angular size these yield  $n_{\text{H}_2} \sim 1.3 \times 10^5 \text{ cm}^{-3}$  and  $N_{\text{H}_2} \sim 4 \times 10^{23} \text{ cm}^{-2}$ . We note these parameters are similar to those derived by Garay et al. (2004) who made use of just the 1.2-mm flux, com-

bined with upper limits at 60 and 100- $\mu\text{m}$  from IRAS data – yielding an upper limit to the temperature of 17-K. Thus, the dust-determined temperature is comparable to that derived from the  $\text{NH}_3$  emission, giving us confidence in the conclusion that the core is exceedingly cold. If we assume that the molecular lines are thermalized then  $T_{\text{kin}}$  is approximately equal to the excitation temperature ( $T_{\text{ex}}$ ) for each molecule.

Most of the detected molecular lines are peaked at  $\sim -57 \text{ km s}^{-1}$ , except for  $\text{HCO}^+$ , HNC and  $\text{N}_2\text{H}^+$  which are peaked at  $\sim -59 \text{ km s}^{-1}$ . This likely due to lines being optically thick, for instance the  $\text{H}^{13}\text{CO}^+$  line peaks at  $-57 \text{ km s}^{-1}$ . The methanol maser also peaks at  $-57 \text{ km s}^{-1}$ , with components at  $-53$  and  $-63 \text{ km s}^{-1}$  (Ellingsen 2005), indicative of outflows. The water maser is at  $-54 \text{ km s}^{-1}$ . The line widths for most of the molecules are between 3 to  $5 \text{ km s}^{-1}$  as opposed to the  $\sim 0.5 \text{ km s}^{-1}$  predicted for quiescent gas dominated by thermal broadening, suggesting the core is turbulent. The SiO however has the largest line width amongst the detected molecular lines,  $9.0 \pm 1.1$



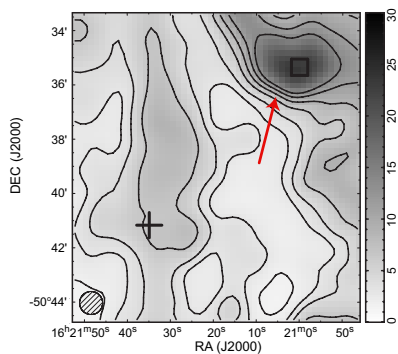


**Figure 4.** The integrated emission map of  $^{13}\text{CO}$  ( $J = 1 \rightarrow 0$ ) from  $-52$  to  $-50 \text{ km s}^{-1}$ . The contour levels are 0.6, 1.8, 3.0, 4.2, 8.8, 9, 11.4 and  $13.8 \text{ K km s}^{-1}$ . The temperature is in terms of the antenna temperature,  $T_{\text{A}}^*$ . The cross marks the cold core G333.125–0.562 and the square marks IRAS 16172–5028. The arrow indicates a likely region where the gas is being compressed.

$\text{km s}^{-1}$ , leading further support to being associated with an outflow. Its abundance with respect to  $\text{H}_2$  has an upper limit of  $\sim 10^{-12}$  in quiescent gas, but is greatly enhanced in powerful shocks, up to  $\sim 10^{-7}$  (e.g. Ziurys, Friberg & Irvine 1989; Martin-Pintado, Bachiller & Fuente 1992). We have determined the abundance to be  $\sim 10^{-9}$ , in between these extremes. A similar abundance ratio has been found in molecular outflows, e.g. Codella, Bachiller & Reipurth (1999), Garay et al. (2002). A follow up  $^{12}\text{CO}$  ( $J = 1 \rightarrow 0$ ) molecular line observation over a five square arcmin region of the core was taken in June 2007, the spectra clearly shows line wings, however they are confused with multiple velocity components and needs further investigation.

#### 4 WHAT IS GENERATING THE SiO EMISSION: OUTFLOWS OR COLLISIONS?

The optically thick isotopomers clearly show two different velocity components, indicating there are two separate clouds in this region. The cloud at  $\sim -50 \text{ km s}^{-1}$  is associated with IRAS 16172–5028, and is at the ambient velocity of G333 giant molecular cloud (see Figure 3l). The other cloud at  $\sim -58 \text{ km s}^{-1}$  is associated with the cold core G333.125–0.562 (Figure 3k). The SiO emission could be generated by these two clouds colliding, but we consider this unlikely. First, consider the confined emission of the SiO, localised to the dust core itself. If it is due to a cloud-cloud collision we would expect more extended distribution. Secondly, for a cloud-cloud collision there should be distinctive features in the density structure. Shown in Figure 4 is the  $^{13}\text{CO}$  integrated emission map of velocity range  $-52$  to  $-50 \text{ km s}^{-1}$ . Note the sharp edge (arrow) on the left side of the IRAS source (square), suggesting compression of the gas here. However no compression is evident associated with the cold core (cross) at the velocity observed.

#### 5 SUMMARY AND CONCLUSION

From our molecular line survey of the G333 Giant Molecular Cloud, we have detected thermal SiO emission from the

massive, cold, dense core, G333.125–0.562, with an abundance enhanced over typical unshocked molecular cloud values. This core has a gas mass of  $1.8 \times 10^3 M_{\odot}$ , is undetected up to  $70\text{-}\mu\text{m}$  and has compact 1.2-mm dust continuum emission. From the  $\text{NH}_3$  inversion lines we derived a temperature of 13 K, which is comparable with that derived from the SED (19 K). The detection of compact emission from a cold gas tracer ( $\text{N}_2\text{H}^+$ ) suggests this is a dense cold core. Typical line widths are between 4 to  $5 \text{ km s}^{-1}$ , indicating the core is turbulent, as expected in massive star formation.

In conclusion, from these observations we believe that the cold massive core harbours a deeply embedded, massive protostellar object that is driving an outflow. This is occurring at a very early stage of star formation, prior to the creation of an infrared source in the core.

#### ACKNOWLEDGMENTS

The Mopra Telescope is part of the Australia Telescope and is funded by the Commonwealth of Australia for operation as National Facility managed by CSIRO. The University of New South Wales Digital Filter Bank used for the observations with the Mopra Telescope was provided with support from the Australian Research Council. We would like to thank the reviewer's constructive comments on improving this paper, T. Wong for his work on  $\text{C}^{18}\text{O}$  data, and S. N. Longmore for help in analysing the  $\text{NH}_3$  data. This research (GLIMPSE and MIPS GAL images) has made use of the NASA/IPAC Infrared Science Archive which is operated by the Jet Propulsion Laboratory, California Institute of Technology, under contract with NASA. The molecular line rest frequencies are from Lovas, Johnson & Snyder (1979).

#### REFERENCES

- Bains I., Wong T., Cunningham M., Sparks P., Brisbin D., Calisse P., Dempsey J. T., Deragopian G., et al., 2006, MNRAS, 367, 1609
- Codella C., Bachiller R., Reipurth B., 1999, A&A, 343, 585
- Danby G., Flower D. R., Valiron P., Schilke P., Walmsley C. M., 1988, MNRAS, 235, 229
- Ellingsen S. P., 2005, MNRAS, 359, 1498
- Ellingsen S. P., von Bibra M. L., McCulloch P. M., Norris R. P., Deshpande A. A., Phillips C. J., 1996, MNRAS, 280, 378
- Faúndez S., Bronfman L., Garay G., Chini R., Nyman L.-Å., May J., 2004, A&A, 426, 97
- Garay G., Faúndez S., Mardones D., Bronfman L., Chini R., Nyman L.-Å., 2004, ApJ, 610, 313
- Garay G., Mardones D., Rodríguez L. F., Caselli P., Bourke T. L., 2002, ApJ, 567, 980
- Hill T., Thompson M. A., Burton M. G., Walsh A. J., Minier V., Cunningham M. R., Pierce-Price D., 2006, MNRAS, 368, 1223
- Hirota T., Yamamoto S., Mikami H., Ohishi M., 1998, ApJ, 503, 717
- Hotzel S., Harju J., Walmsley C. M., 2004, A&A, 415, 1065
- Karnik A. D., Ghosh S. K., Rengarajan T. N., Verma R. P., 2001, MNRAS, 326, 293

- Kim S.-J., Kim H.-D., Lee Y., Minh Y. C., Balasubramanyam R., Burton M. G., Millar T. J., Lee D.-W., 2006, *ApJ Supp*, 162, 161
- Ladd N., Purcell C., Wong T., Robertson S., 2005, *Publ. Astron. Soc. Aust.*, 22, 62
- Lintott C. J., Viti S., Rawlings J. M. C., Williams D. A., Hartquist T. W., Caselli P., Zinchenko I., Myers P., 2005, *ApJ*, 620, 795
- Lovas F. J., Johnson D. R., Snyder L. E., 1979, *ApJ Supp*, 41, 451
- Martin-Pintado J., Bachiller R., Fuente A., 1992, *A&A*, 254, 315
- Mookerjee B., Kramer C., Nielbock M., Nyman L.-Å., 2004, *A&A*, 426, 119
- Pestalozzi M., Humphreys E. M. L., Booth R. S., 2002, *A&A*, 384, L15
- Ungerechts H., Winnewisser G., Walmsley C. M., 1986, *A&A*, 157, 207
- Womack M., Ziurys L. M., Wyckoff S., 1992, *ApJ*, 387, 417
- Ziurys L. M., Friberg P., Irvine W. M., 1989, *ApJ*, 343, 201

This paper has been typeset from a  $\text{\LaTeX}$  file prepared by the author.